15th Seminar "New Trends in Research of Energetic Materials", Part II, pp. 881-892, ISBN 978-80-7395-480-2, University of Pardubice, Pardubice, Czech Republic, April 18–20, 2012.

Numerical simulation of internal ballistics parameters of solid propellant rocket motors

Jasmin Terzic, Berko Zecevic, Sabina Serdarevic-Kadic, Alan Catovic

University of Sarajevo, Mechanical Engineering Faculty, Sarajevo, Bosnia and Herzegovina

terzic@mef.unsa.ba

Abstract:

During the initial phase of design of solid propellant rocket motors it is necessary to identify and quantitatively estimate deviation of internal ballistics parameters of observed rocket motors types from ideal conditions. In an initial stage of the design of real rocket motors there are differences between the rocket motor theoretical performances and actual performances based on testing of standard ballistic motors.

Therefore modern numerical methods were used as a potential tool for the analysis of characteristics of combustion and gas flow in solid propellant rocket motors with specific design. Numerical simulations provide analysis of certain physical processes in rocket motors, optimizing and reducing the cost of development of new rocket systems (minimizing number of models and tests).

Mathematical and numerical 3D model, based on equations of mass, momentum and energy conservation, describing transport processes in rocket motors, is used. Numerical simulation in CFD package Comet (finite volume method) was con-ducted for real gas flow through the passage channel (for propellant charge gasses), and in the front and along the nozzle.

The results of numerical simulations were verified with theoretical solution for the case of quasi-steady combustion process, with available experimental data of other authors and with our own experimental studies.

Keywords: rocket motors; burning rate; numerical model; compressible flow; transonic flow; boundary conditions; mass flow rate; burning surface.

1 Introduction

Most of the existing models for predicting of internal ballistics performance solid propellant rocket motors are based on the one-dimensional (1D) mathematical models for solving the basic equations of fluid mechanics, which are equations of continuity and momentum equations. The one-dimensional models are used in the commercial applications, such as *SPP* (Solid Performance Program), SNIA-BPD (Bombrini Parodi-Delfino S. p. A.), Defense and Space Division, Colleferro, Italy [11-13,16,18], and their advantage is a speed in problem solving. The *SPP* program is used by leading manufacturers of solid propellant rocket motors on in the USA and several other countries. This program allows the prediction and/or performance analysis of hundreds of different rocket motors, but unfortunately, most of these data are generally not available for most countries [12].

Modern numerical methods are potential tools for the analysis of fluid flow characteristics of the solid propellant rocket motor. Modern examples of application of numerical methods for modeling flow in solid propellant rocket motors are presented in the studies of the Center for Simulation of Advanced Rockets, Sachadev, Ciucci and co-authors [1-10,14,15]. In these works, the prediction of the 2D axial-symmetric and 3D non viscous fluid flow, takes into account the development of the area between the propellant and combustion products flow as

well as the multiphase flow of gas in the inner cavity propellant grain. Simulations were extended to the analysis of viscous, turbulent gas flow and the simulation of solid propellant rocket motor during operation in the normal and the abnormal operating conditions.

Since September 1997, the Center for Simulation of Rocket Advanced (CSAR), the University of Illinois at Urbana-Champaign, for the needs of Department of Energy, develops the program for predicting the performance of rocket motors with solid propellants based on a numerical simulation [1-6,8,9,17,24]. Their primary objective was to develop models that will allow the numerical simulation of physical processes in the rocket motor, which includes full 3D modeling of reactive, and turbulent multi-phase gas flow, complex geometries and interfaces, for a different length and time scales.

Models that allow the numerical simulation of such problems require high performance computers. There are a number of developed sophisticated computer modules so far for the basic components of rocket motors, as well as the interaction between them in normal and operating conditions (figure 1). All of these modules were compared with the results of experimental rocket motors at a reduced scale and real rocket motors.

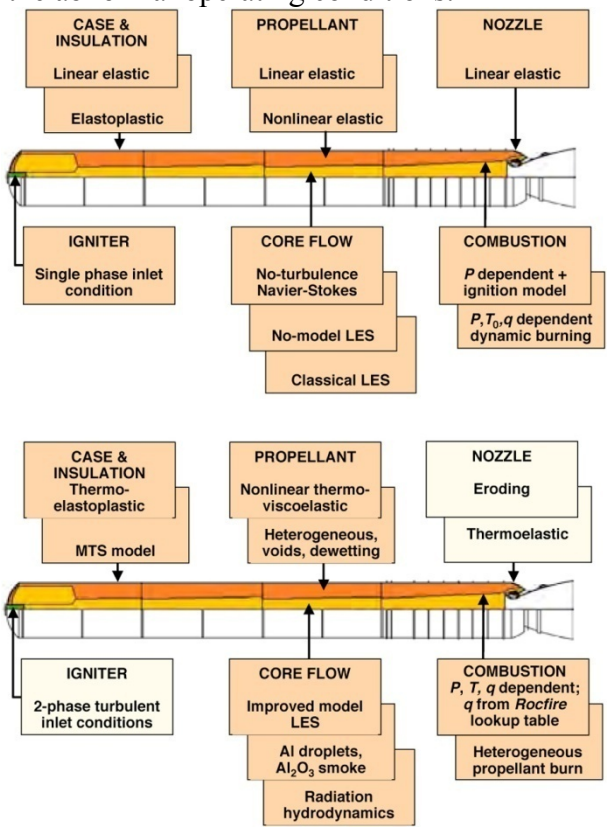

Figure 1: Module development for Rocstar follows path of increasing complexity of physical component models [1]

2 Governing equations and numerical method

To highlight that the same equations of the conservation of mass, momentum and total specific energy can be equally used to describe gas phase as well as solid phase, subjected respectively to the burning of the surface and to very high combustion pressure forces, in three dimensions the equations are written in the general [19], integral form, as

$$\frac{d}{dt}\int_V \rho\, dV + \int_S \rho(\mathbf{v}-\mathbf{v}_s)\cdot d\mathbf{s} = 0 \tag{1}$$

$$\frac{d}{dt}\int_V \rho\,\mathbf{v}\, dV + \int_S \rho\,\mathbf{v}(\mathbf{v}-\mathbf{v}_s)\cdot d\mathbf{s} = \int_S \mathbf{T}\cdot d\mathbf{s} + \int_V \rho\mathbf{f}_b dV \tag{2}$$

$$\frac{d}{dt}\int_V \rho\, E dV + \int_S \rho\, E(\mathbf{v}-\mathbf{v}_s)\cdot d\mathbf{s} = -\int_S \mathbf{q}_h\cdot d\mathbf{s} + \int_V s_h dV + \int_V \mathbf{T}{:}grad\,\mathbf{v}\, dV \tag{3}$$

where are: t - time, ρ - density of continuum, $\mathbf{v}$ - continuum velocity vector, $\mathbf{v}_s$ - surface velocity vector, $\mathbf{s}$ - outward pointing surface vector, $\mathbf{T}$ - Cauchy stress tensor, $\mathbf{f}_b$ - resultant body force per unit volume, E - total energy (is the sum of the specific internal or thermal energy e, specific mechanical energy $\mathbf{v}^2/2$), $\mathbf{q}_h$ - heat flux vector and s_h - heat source.

Equations (1) to (3) consists of an open system and for their closure, it is necessary to define the appropriate constitutive relations that provide a link between stress and heat flux, on

the one hand, and the incremental displacement vector, velocity vector and temperature, on the other hand:

- Stokes' law - Relation between stresses **T** and the rate of deformation $\dot{\mathbf{D}}$ for fluids:

$$\mathbf{T} = 2\mu\,\dot{\mathbf{D}} - \frac{2}{3}\mu \mathrm{div}\,\mathbf{v}\mathbf{I} - p\mathbf{I}\,, \tag{4}$$

where

$$\dot{\mathbf{D}} = \frac{1}{2}\left[grad\ \mathbf{v} + (grad\ \mathbf{v})^T\right]. \tag{5}$$

is the rate of strain tensor, μ is the dynamic viscosity, p is the pressure and **I** is the unit tensor.

- Fourier's law

$$\mathbf{q}_\mathrm{h} = -k\,\mathrm{grad}T \tag{6}$$

where are: $\mathbf{q}_\mathrm{h}$ - heat flux, k - thermal conductivity.

- Equations of state

$$\rho = \rho(p,T), \quad e = e(p,T). \tag{7}$$

Common examples are, e.g $\rho=const.$, $e=C_vT$ (for incompressible fluids and solids) or $\rho=p/(RT)$, $e=C_vT$ (for an ideal gas). Here C_v is the specific heat at constant volume and R is the gas constant.

Inclusion of constitutive relations (4) to (7) into the basic balance equations of mass, momentum and energy (1) to (3) gives a closed system of three equations with three unknown functions (e, p, v) of the spatial coordinates and time. The equations of momentum and energy can be written as the following general transport equation:

$$\frac{\mathrm{d}}{\mathrm{d}t}\int_V \rho B_\phi \mathrm{d}V + \int_S \rho\phi(\mathbf{v}-\mathbf{v}_\mathrm{s})\cdot\mathrm{d}\mathbf{s} = \int_S \Gamma_\phi \mathrm{grad}\phi\cdot\mathrm{d}\mathbf{s} + \int_S Q_{\phi S}\cdot\mathrm{d}\mathbf{s} + \int_V Q_{\phi V}\mathrm{d}V \tag{8}$$

where ϕ can be thermal energy, velocity vector, while the equation of continuity is usually combined with equation of motion to determine the pressure. The meaning of the quantities B_ϕ and Γ_ϕ, in the case of basic constitutive relations and turbulent flow, are given in Table 1. The term $Q_{\phi S}$ contains portions of the mass or heat flux vector or the stress tensor which are not contained in $\Gamma_\phi \mathrm{grad}\phi$, while $Q_{\phi V}$ contains the volumetric source terms.

Table 1: The meaning of various terms in the generic transport equation (8)

ϕ	B_ϕ	Γ_ϕ	$Q_{\phi V}$	$Q_{\phi S}$
e	e	k	$\mathbf{T}:\mathrm{grad}\mathbf{v} + s_\mathrm{h}$	0
v	**v**	μ	$\rho\mathbf{f}_\mathrm{b}$	$\mu(\mathrm{grad}\mathbf{v})^\mathrm{T} - \left(\frac{2}{3}\mu\mathrm{div}\mathbf{v} + p\right)\mathbf{I}$

However, before a solution of the generic transport equation (8) is attempted, several important decisions have to be made, concerning: the choice of vector and tensor components, the space and time discretization procedure, and the variable storage arrangement.

An appropriate decision about these options is decisive for the stability, conservativeness, and efficiency of the numerical method. In *Comet*, the following choices are made:

- Although the analysis is carried out in a coordinate-free (invariant) form (which enables any vector and tensor components to be used), vectors and tensors will be expressed through their Cartesian components. They lead to a strong conservation form of all equations (including momentum equation), and the method is not sensitive to mesh smoothness.

- The space is discretized by an unstructured mesh with polyhedral control volumes (CVs). In order to allow the greatest exibility in adapting the mesh to complex 3D geometries, polyhedra with any number of sides ($n \geq 4$) are allowed, and cells of different topology may be used in the same problem. As far as time discretization is concerned, the time interval of interest is subdivided into an arbitrary number of subintervals (time steps), not necessarily of the same duration.
- All dependent variables are stored at the cell center.

Equation (8), when written for the control volume, gets the following form:

$$\frac{\mathrm{d}}{\mathrm{d}t}\int_V \rho B_\phi \mathrm{d}V + \sum_{j=1}^{n}\int_S \rho\phi(\mathbf{v}-\mathbf{v}_s)\cdot\mathrm{d}\mathbf{s}_j = \sum_{j=1}^{n}\int_S \Gamma_\phi \mathrm{grad}\phi\cdot\mathrm{d}\mathbf{s}_j + \sum_{j=1}^{n}\int_S Q_{\phi S}\cdot\mathrm{d}\mathbf{s}_j + \int_V Q_{\phi V}\mathrm{d}V \quad (9)$$

where n is the number of faces enclosing the CV. Equation (9) has four distinct parts: transient rate of change, convection, diffusion and sources. This equation is exact, i.e. no approximation has been introduced so far. However, in order to evaluate integrals in the above equation, the following steps need to be performed:

- generation of a numerical grid and calculation of geometric data needed for evaluation of surface and volume integrals,
- choice of quadrature approximations for surface and volume integrals,
- choice of interpolation functions for spatial distribution of variables,
- choice of numerical differentiation approximations,
- choice of time integration scheme,
- some means of determining surface velocities $\mathbf{v}_s$ have to be provided.

These steps are described in reference [19].

2.1 Implementation of boundary conditions

In discussing the process of rocket propellant combustion and the flow of combustion products through the inner channel of the propellant grain and the nozzle of the rocket motor; the following boundary conditions may appear (Figure 2) [9,20]:

- At the inlet region (for the steady state is considered only a gas supply created during the combustion of propellant grain, while for the unsteady state must be considered the process of regression of the propellant grain)
- At the Outlet region,
- Symmetry plane and
- On the wall (the base of rocket motor, chamber of combustion and the nozzle).

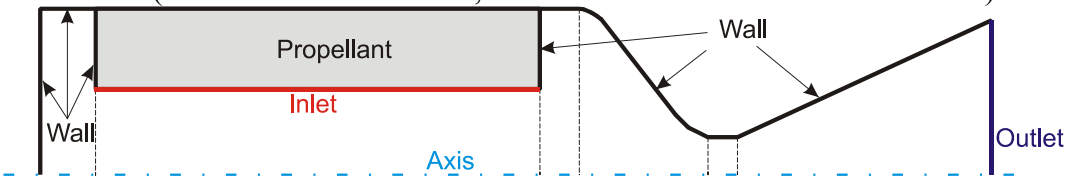

Figure 2: Scheme of boundary conditions of the solid propellant rocket motor

In the case of compressible and transonic flow (occurring during the flow of gas in the chamber of combustion in the nozzle of motor), a software package *Comet* proposes the following combination of boundary conditions for the case of inlet and outlet flow [19]:

- The inlet region is subsonic and the outlet region is subsonic/supersonic:
  - The inlet flow can be considered by: defining total conditions at the inlet or the conditions of mass flux on the burning surface.
  - The outlet flow can be considered only if the pressure conditions are defined at the outlet region.

2.1.1 Inlet boundaries

In the simulation of solid propellant combustion, combustion chamber pressure is a function of the mass burning rate of propellants (depending on the burning area, burning rate and density of propellants) and the mass outflow rate of combustion products through the critical nozzle section (function of pressure in the combustion chamber and the throat area and the coefficient of the mass flow rate). Such complex interdependence of these parameters cannot be defined by placing the total conditions on inlet region but it is only possible to simulate the mass flow rate through the inlet region.

Based on the theoretical and experimental studies, we can assume that the combustion process is completed in the combustion zone, which is, compared to the entire rocket motor considered as a surface between the propellant grain and the gas flow of very small thickness, which is negligible thickness (Table 2). The final composition of combustion products, originating from combustion of the propellant is most probably established on the burning area, therefore this boundary region is considered as inlet region.

Table 2: Characteristics of the Combustion Zones for double base propellant [21,22]

Pressure, MPa	1	5	10
Burning rate, mm/s	1,9	6,7	10,6
Temperature of burning surface, K	610	662	685
Preheated zone (measured/computed), μm	140/194	50/55	45/35
Residence time in preheated zone, ms	100	8	3
Superficial degradation zone, μm	11	3	2
Residence time in superficial zone, ms	6	0,5	0,2
Flame thickness (measured), μm	200	75	110 (secondary flame)

When analyzing the combustion process in this model, it is considered that the burning rate depends only on the combustion pressure and it is determined based on the equation:

$$r_b = a \cdot p^n \qquad (10)$$

Figure 3 shows the combustion boundary between the propellant grain (solid domain) and the combustion products (gas domain). This boundary moves with burning rate r_b and it is normal to the burning surface of the propellant grain.

The combustion products are leaving the burning surface at a velocity that is significantly greater than the burning rate. The velocity of combustion products was determined on the basis of the conservation of mass law [23, 24]:

$$\rho_p \cdot r_b \approx \rho_g \cdot \mathbf{v}_B \qquad (11)$$

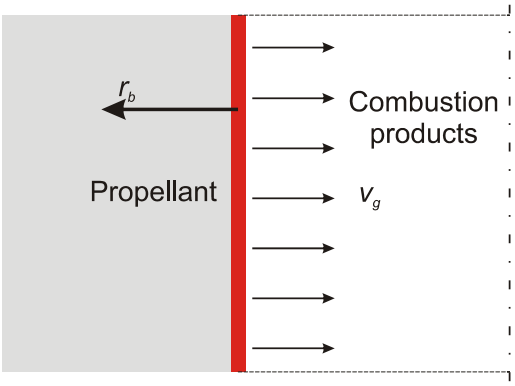

Figure 3: Injection conditions on the combustion surface

where: ρ_p and ρ_g – are density of propellant or combustion products, r_b - burning rate and $\boldsymbol{v_B}$ – vector of velocity of combustion products.

Density of combustion products we determine from the equation of state:

$$\rho_g = \frac{p_B}{R_g \cdot T_B} \qquad (12)$$

where: p_B is a pressure on the inlet region which is obtained by extrapolation from internal grid, T_B is temperature at the inlet region and it is assumed to be equal to the combustion temperature for a given propellant composition and R_g is a gas constant.

In this analysis we will use known thermo physical and thermo chemical parameters of the double base propellant combustion products obtained on the bases of the model *TCPSP* [25, 26].

Assuming that the burning rate is function of the pressure only, we obtain an expression for the velocity of combustion products in the inlet region:

$$\mathbf{v}_B = -\frac{\rho_p \cdot a \cdot p_B^n}{\rho_g} \cdot \mathbf{c}_B \tag{13}$$

For simulation of deformation and regression of burning surface, component of the gas velocity are relative to burning surface. Assuming that the propellant grain burns on parallel layers, normal to the surface of the combustion flame, surface regression is determined on the basis of the expression [6,27]:

$$x_{new} = x_{old} + (r_b)_x \cdot \delta t \tag{14}$$

$$r_{new} = r_{old} + (r_b)_r \cdot \delta t \tag{15}$$

where x and r are cylindrical coordinates, $(r_b)_x$ and $(r_b)_r$ are corresponding components of burning rate.

2.1.2 Outlet - Pressure boundaries

The pressure boundary conditions can be specificed on that portion of boundary where the pressure distribution is known. At pressure boundaries the prescribed boundary pressure $p(\mathbf{r}_B,t)$ is combined with the Neumann boundary condition [19]:

$$\frac{\partial \mathbf{v}}{\partial n} = 0 \,. \tag{16}$$

to obtain boundary velocities $\mathbf{v}_B(\mathbf{r}_B,t)$.

If the zero pressure gradient can be assumed at a certain portion of the boundary, than the pressure at the boundary can be approximated as

$$p(\mathbf{r}_B,t) = p(\mathbf{r}_{P_0},t), \tag{17}$$

where P_0 is the center of the control volume next to the boundary.

2.1.3 Symmetry boundaries

In many practical situations the problem exhibits some kind of symmetry in which case only one part of the (fluid or solid) body may be taken as the solution domain and the symmetry plane boundary conditions, which are a combination of Dirichlet and Neumann boundary conditions, are applied.

For velocities the following conditions apply [19]:

$$\mathbf{v}_{B_n}(\mathbf{r}_B,t) = 0 \,, \quad \frac{\partial \mathbf{v}_{B_t}(\mathbf{r}_B,t)}{\partial n} = 0 \tag{18}$$

where $\mathbf{v}_{B_n}$ and $\mathbf{v}_{B_t}$ are the velocity components normal and tangential to the boundary respectively $\mathbf{v}_B = \mathbf{v}_{B_n} + \mathbf{v}_{B_t}$.

For all scalar variables, for example for temperature, the simple Neumann boundary conditions apply:

$$\frac{\partial T(\mathbf{r}_B,t)}{\partial n} = 0 \tag{19}$$

2.1.4 Wall boundaries

This boundary condition is applied at the boundaries of the rocket motor case: base, combustion chamber and the nozzle as well as on the boundaries of propellant grain that does not burn. This boundary condition can be considered in two ways:

- Slip wall. If the sheer force at the wall is negligible in comparison to other forces, the wall can be considered as a slip wall. The typical situations where this assumption holds are inviscid and high-Mach number flows, where the momentum transport due to molecular viscosity is negligible compared to the convective transport.
- No-slip wall. However, these are idealized situations, and the no-slip wall boundary conditions are used in most practical situations. The no-slip boundary condition at a wall can be specificed by prescribing the values of velocity or the force exerted by the wall.

The mass flux through an impermeable wall is zero and the pressure is always extrapolated to the boundary from inside the solution domain.

3 Results

The testing of developed numerical method was performed by program package *Comet* on the examples of compressible flow using recommended boundary conditions for this type of flow. For testing of model examples were used from numerical solutions of other related programs for simulation of internal ballistic parameters of the rocket motor as well as experimental results.

In order to illustrate the applicability and the efficiency of the method, the several test examples were checked, including simulation of axial symmetrical flow of gas inside the rocket motor for two configurations: internal-external burning tube grain and internal burning tube grain. Dimensions of rocket motor and characteristics of the combustion products of double base propellant NGR-A are given in table 3.

Table 3: Characteristics of rocket motors and propellant NGR-A

Type of rocket motors	32/16	128 mm
Length of combustion chamber, mm	133	526.5
Diameter of combustion chamber, mm	39.2	119.8
Diameter of propellant grain, mm	32	119.8
Internal diameter of propellant grain, mm	16	63.3
Length of propellant grain, mm	125	500
Diameter of throat area, mm	11	29.4
The nozzle-divergence half-angle	13°	11°
Density of propellant, kg/m^3	1600	
Specific heat of propellant, J/(kg K)	1450	
Temperature of combustion, K	2351.0	
Temperature of burning surface, K	650	
Burning rate low, m/s	$0.0130717[p(\mathrm{MPa})]^{0.227587}$ for $p_c<14$MPa, $0.0216156[p(\mathrm{MPa})]^{0.036981}$	
Specific heat of gasses, J/(kg K)	1814.2	
Gas constant, J/(kg K)	344.	
Thermal conductivity, W/mK	0.1853	
The molar mass, g/mol	24.183	
The ratio of specific heat	1.2463	

3.1 Standard ballistic rocket motor 32/16

The first case of numerical simulation we considered the gas flow in a standard ballistic rocket motor 32/16 with internal-external burning tube grain. The radius of curve from the convergent part of nozzle to the critical section is 4.75 mm. Two-dimensional axial-symmetric spatial domain is divided into 4400 CV with a non uniform mesh (Fig. 4).

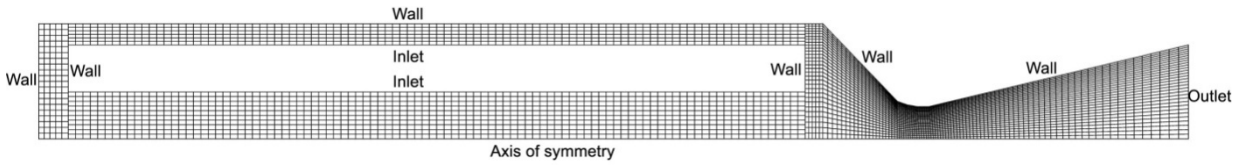

Figure 4: Numerical grid and boundary conditions for example of rocket motor 32/16

The propellant grain burns from all sides, so if we ignore burning from the front and back side of the grain, the burning area during remains constant over time. The initial burning area is A_b= 0.01884956m^2, and the throat area is A_t= 9.50332E-05m^2. We have investigated the combustion of double base propellant NGR-A (Table 3).

The results of numerical simulations were compared with a theoretical solution for the case of quasi-stationary combustion process. The value of equilibrium pressure at the plateau can be estimated from the equilibrium of mass rates for gases generated in the combustion chamber and gases leaving the nozzle:

$$p_c = \left(\frac{\rho_p \cdot a \cdot A_b}{C_D \cdot A_t} \right)^{\left(\frac{1}{1-n}\right)} \tag{20}$$

Equation (20) is valid if the magnitude of the time rate of change of chamber pressure is low enough to cause an insignificant effect on propellant ballistic characteristics, and the pressure over the entire burning surface is essentially constant. This equation does not consider transient period of combustion until the value of equilibrium pressure is achieved.

Results of the numerical simulation compared to the theoretical solutions for 0-D equation of mass balance which considers pressure change over time. The chamber pressure is assumed to be uniform throughout the rocket chamber; therefore, the burning rate is uniform as well. Assuming the temporal derivative of chamber volume to be negligible and the gas temperature to be constant at the adiabatic flame temperature. Based on these assumptions and using equation of mass balance in the rocket motor, the combustion pressure can be calculated with following equation, by Runge-Kutta method of 4th order:

$$\frac{dp_c}{dt} = \frac{R_g \cdot T_c}{V_c} \cdot \left(\rho_p \cdot A_b \cdot a \cdot p_c^n - \frac{p_c \cdot A_{th}}{C^*} \right) \tag{21}$$

Results of comparison between numeric model (*Comet*) and theoretical model, given in equation (21) are shown in Fig. 5. Presented change of the pressure in the function of time obtained by numerical simulation is given for the base of the rocket motor in the axis of rocket motor and the equilibrium state is achieved after 0.06758 s.

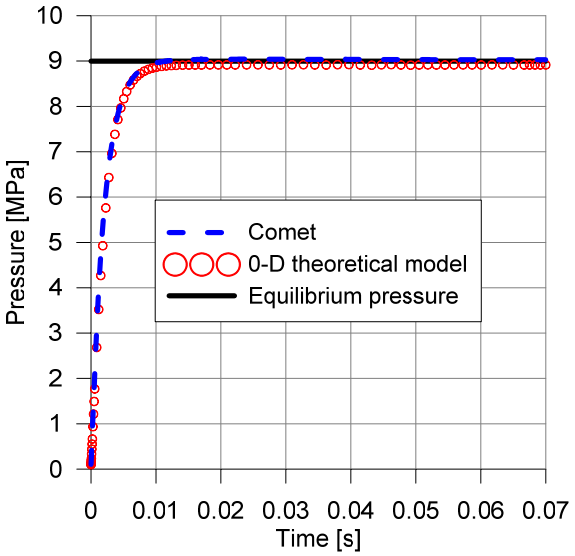

Figure 5: Comparison of results of changes p=f(t) obtained by numerical simulation and theoretical results for the rocket motor 32/16

Results of numerical model and theoretical solutions have good agreement. The value of equilibrium pressure obtained by numerical simulation p_c=9.047 MPa is very close to the value of the equilibrium pressure obtained by equation (20), p_c=8.998 MPa is slightly lower with the value p_c=8.925 MPa.

Deviations of solutions based on the numerical simulation compared to equilibrium pressure obtained by equation (20) is around 0,55% while deviation of results obtained by equation (21) is around 0,8%.

3.2 Simulation of the regression of burning surface

Obtained results show very good agreement with theoretical models for the steady state, which means no changes of burning surface. During the work of the rocket motor, when combustion of propellant grain takes place, the burning area is changing as well as the surface of channel for the passage of gas and that contributes to the change of the flow field inside the chamber of rocket motor. Numerical simulation of regression of burning surface was conducted and results were compared to results from program *SPPMEF* [25,28].

We considered the same rocket motor as in the previous case, and in the process of numerical simulation of the burning surface regression, we considered displacement of the inlet regions only in the radial direction (outer radius of the grain decreases, and the inner radius increases). With assumption that the propellant grain burns on parallel layers, normal to the burning surface, burning surface regression is determined from expression:

$$r_{in_{new}} = r_{in_{old}} + r_b \cdot \delta t$$
$$r_{out_{new}} = r_{out_{old}} - r_b \cdot \delta t \qquad (22)$$

In determination of the burning rate in the previous formula, we used average value of the pressure of combustion on the surface of the inlet region. In both cases of simulation, we used the same assumptions for the process of combustion and combustion surface displacements. The results of comparison between the numerical model (*COMET*) program and *SPPMEF* are shown in Figure 6.

There is a very good matching in predicting the change of the pressure with the time and the data obtained by prediction based on program *SPPMEF*.

The deviation values of the integral of pressure-time are 0.98% and the maximum pressure is 0.7% compared to the results of prediction of program *SPPMEF*.

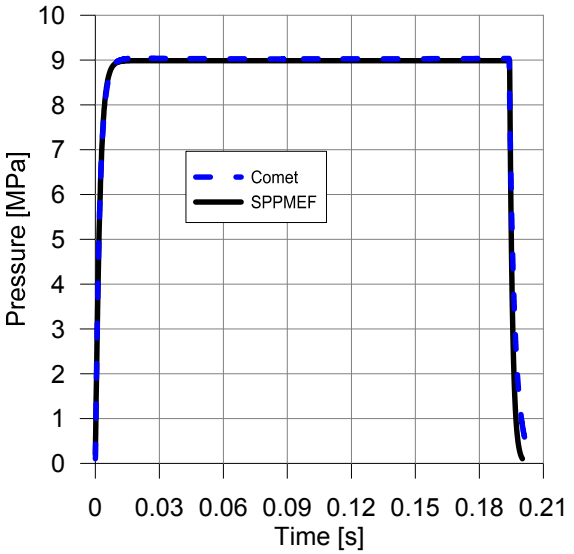

Figure 6: Comparison of results of changes p=f(t) obtained by numerical simulations and program *SPPMEF* for the rocket motor 32/16.

The time required to simulate the pressure change in the function of time in the software package *Comet* was about 140 minutes and for the program *SPPMEF* about 2 minutes on a PC (Core 2 Duo processor 2.4MHz, 3GB RAM). Program *SPPMEF* enables prediction of average performances such as mass flux, pressure, thrust and specific impulse as a function of time. Software package *Comet* enables numerical simulation of 3D gas flow parameters, and with developed modules for regression of burning surface and internal ballistics parameters of rocket motor, it is possible to simulate influence of rocket motor geometry on change of pressure (on different places in combustion chamber) and thrust as a function of time.

3.3 Experimental rocket motor 128 mm

This rocket motor has internal burning tube grain (dimensions given in Table 3). The radius of curvature of the nozzle profile in the critical section of the nozzle is 30 mm.

Two-dimensional axial-symmetric spatial domain is divided into 21350 CV with a non uniform mesh (Fig. 7).

Assuming that the propellant grain burns on parallel layers, normal to the surface of combustion, burning surface regression is determined on the basis of the expression:

$$r_{in_{new}} = r_{in_{old}} + r_b \cdot \delta t \quad \textbf{(23)}$$

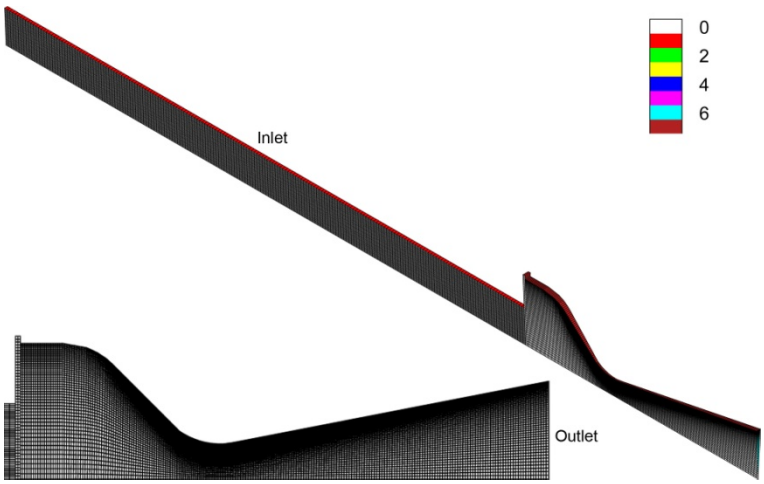

Figure 7: Numerical grid and boundary conditions for the rocket motor 128 mm

The data obtained in numerical simulation (*COMET*) and the program *SPPMEF* are shown in Figure 8.

Good agreement was achieved in the prediction of change in pressure with the time.

The deviation values of the integrals of the pressure-time are 0.55% compared to the results of prediction of *SPPMEF*. The values of the maximum pressure are almost identical.

The time required to simulate the pressure change in the function of time in the software package *Comet* was about 43 hours (on the PC, processor Core 2 Duo 2. 4MHz, 3GB RAM).

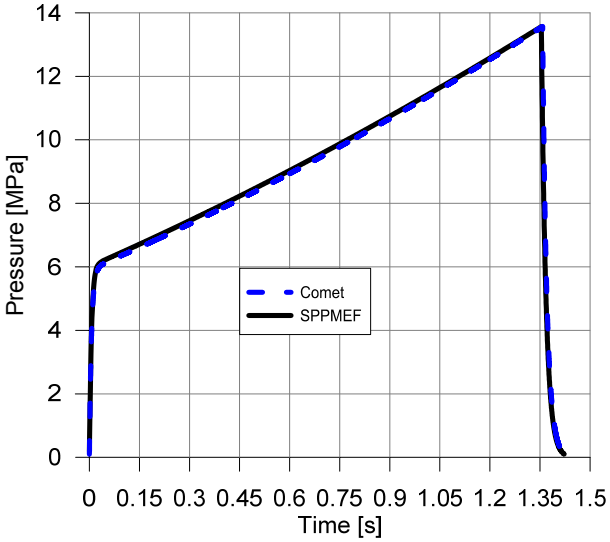

Figure 8: Comparison of changes in pressure in the combustion chamber as a function of time between the numerical model (*COMET*) program and *SPPMEF* for the rocket motor 128 mm

3.4 Verification of simulation results with experimental results

Prediction of pressure change in the function of the time by using numerical simulations for 2D axial-symmetric model is verified in such way that the calculation results are compared with experimental results obtained in the standard ballistic rocket motor 32/16. Appropriate operating pressure for combustion is achieved by changing the diameter of the critical nozzle section (no erosion of the critical nozzle cross section). This rocket motor is designed in such way to avoid the erosive burning. During the experiment only a change of pressure in the function of time was measured and following parameters were obtained: average value of combustion pressure, maximum combustion pressure and the integral of the pressure - time.

Figure 9 gives comparison results of change of the pressure with the time, obtained by assumptions based on model of numerical simulation – *Comet* (without correction of burning rate) and obtained by experiment for propellant NGR-A.

Very good agreement of the results of the pressure changes with the time in numerical simulations compared to experiments was achieved. Excellent agreement of the pressure change with the time in the quasi-steady burning phase was achieved, while there are significant differences of pressure change as a function of time in the phase of discharge. The change of pressure with time at the stage of discharge in the model does not consider the remains of unburned propellant, which certainly occurs in real rocket motors.

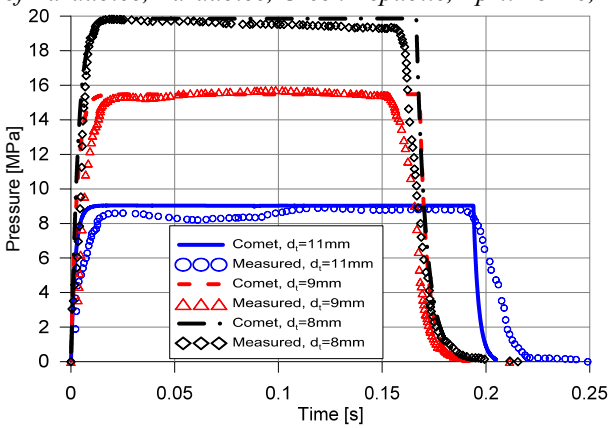

Figure 9: Comparison of changes in pressure in the combustion chamber between the numerical model (*Comet*) and experimental results for the rocket motor 32/16

4 Conclusion

We defined mathematical and numerical model which allows numerical simulation of the regression of propellant grain and transonic flow of combustion products within the solid propellant rocket motor without condensed and solid particles in gas flow.

Authors used *COMET* software package, developed to solve the problem of Newtonian fluids flow, analysis of thermal-elastic deformations and interaction of Newton's fluid and solid body of a linear elastic material, based on finite volume method.

During the verifying of method, we compared the results of simulation using the developed numerical model with the results obtained from analytical solution, experimental tests and results using other methods. We found a very good agreement of the results.

Directions for further research:

- Define a numerical model that will allow the numerical simulation of physical processes in the rocket motor, which include full 3D modeling of reactive, turbulent and multi-phase gas flow, of complex geometries and interfaces, for a different length and time scales. Models that allow the numerical simulation of such problems require high performance computers.
- Define a model, capable to examine the ignition process and the change of pressure and mass flow rate of ignition as the function of time.
- Define a numerical model that will allow assessment of the structural integrity of the rocket motors, and particularly the propellant of complex configuration and the channels for the passage of gases.

References

[1] 2005-6 Annual Report, Center for Simulation of Advanced Rockets, University of Illinois at Urbana-Chamaign, Urbana, Illinois 61801, November **2006**

[2] 2003-4 Annual Report, Center for Simulation of Advanced Rockets, University of Illinois at Urbana-Chamaign, Urbana, Illinois 61801, November **2004**

[3] 2002-2003 Annual Report, Center for Simulation of Advanced Rockets, University of Illinois at Urbana-Chamaign, Urbana, Illinois 61801, December **2003**

[4] 2001-2002 Annual Report, Center for Simulation of Advanced Rockets, University of Illinois at Urbana-Chamaign, Urbana, Illinois 61801, December **2002**

[5] 2000-01 Annual Report, Center for Simulation of Advanced Rockets, University of Illinois at Urbana-Chamaign, Urbana, Illinois 61801, December **2001**

[6] 1998-99 Annual Report, Center for Simulation of Advanced Rockets, University of Illinois at Urbana-Chamaign, Urbana, Illinois 61801, December **1999**
[7] A. Ciucci, G. Iaccarino, R. Moser, F. Najjar and P. Durbin: *Simulation of rocket motor internal flows with turbulent mass injection*, Center for Turbulence Research, **1998**
[8] Alvilli P., Buckmaster J., Jackson T.L. and Short M.: Ignition-transient modeling for solid propellant rocket motors, *36th AIAA/ASME/SAE/ASEE Joint Propulsion Conference and Exhibit*, Huntsville, July 16-19, **2000**.
[9] Alvilli P., Tafti D., Najjar F., The Development of an advanced solid rocket flow simulation, Program ROCFLO, *38th AIAA Aerospace Sciences Meeting and Exhibit*, Reno, **2000**.
[10] C. P. T. Groth and S. A. Northrup: Parallel implicit adaptive mesh refinement scheme for body-fitted multi-block mesh, *17th AIAA Computational Fluid Dynamics Conference, Toronto*, Ontario, Canada, June 6–9, **2005**
[11] Douglas E. Coats, Stuart S. Dunn, Jonathan C. French, Ph.D.: *Performance Modeling Requirements for Solid Propellant Rocket Motors*, Published by CPIA, **2003**.
[12] Dunn S.S. and Coats D.E.: 3-D Grain Design and Ballistic Analysis, *AIAA 97-3340*, Software and Engineering Associates, Inc. Carson City, NV, **1997**
[13] Dunn S.S. and Coats D.E.: Nozzle Performance Predictions Using the TDK 97 Code, *AIAA 97-2807*, Software and Engineering Associates, Inc. Carson City, NV, **1997**
[14] J. S. Sachdev, C. P. T. Groth, and J. J. Gottlieb: *Numerical Solution of a Dilute and Disperse Gas-Particle Flow*, University of Toronto Institute for Aerospace Studies, Canada
[15] J. S. Sachdev, C. P. T. Groth, and J. J. Gottlieb: Parallel AMR Scheme for Turbulent Multi-Phase Rocket Motor Core Flows, *17th AIAA Computational Fluid Dynamics Conference, Toronto*, Ontario, Canada, June 6–9, **2005**
[16] J.C. French, D.E. Coats: Automated 3-D Solid Rocket Combustion Stability Analysis, *AIAA-99-2797, Published by the American Institute of Aeronautics and Astronautics*, **1999**.
[17] R. Fiedler, X. Jiao, A. Namazifard, A. Haselbacher, F. Najjar, I. D. Parsons: Coupled Fluid-Structure 3-D Solid Rocket Motor Simulations, *Published by AIAA*, **2001**.
[18] Scippa S.: *Propellant grain design*, Design Method in Solid Rocket Motors, Paris, **1988**
[19] *COMET*, ICCM GmbH, Hamburg, Germany, **1997**
[20] C.Y. Huang, W. Tworzydlo, J.T. Oden, J.M. Bass, C. Cullen, S. Vadaketh: *Solid Rocket Booster Internal Flow Analysis by High Accurate Adaptive Computational Methods*, NASA, Marshal Space Flight Center, TR-91-05, Huntswille, Alabama, March **1991**.
[21] Zenin A.A.: Structure of Temperature Distribution in Steady-State Burning of a Ballistic Powder Combustion, *Expolsion and Shock Waves Journal*, Vol. 2, No.3, **1966**
[22] G. Lengellé, J. Duterque and J.F. Trubert: *Combustion of Solid Propellants, Internal Aerodynamics in Solid Rocket Propulsion*, RTO Educational Notes EN-023, **2004**
[23] P. Kuentzmann: *Introduction to Solid Rocket Propulsion, Internal Aerodynamics in Solid Rocket Propulsion*, RTO Educational Notes EN-023, **2004**
[24] I. D. Parsons, P. Alavilli, A. Namazifard, A. Acharya, X. Jiao and R. Fiedler: Coupled simulations of solid rocket motors, *AIAA-2000-3456, Published by AIAA*, **2000**
[25] J. Terzic: *Prediction of idealized internal ballistic properties of a rocket motor with DB solid propellant*, Master thesis, University of Sarajevo, **2002**.
[26] J. Terzic, A. Lekic and B. Zecevic: Prediction the Theoretical Interior Ballistic Properties of Solid Propellant Rocket Motors, *6th Seminar "New Trends in Research of Energetic Materials"*, University of Pardubice, pp. 420-435, ISBN 0-7194-543-9 April **2003**.
[27] J Szmelter and P Ortiz: Burning surfaces evolution in solid propellants: a numerical model, *Proc. IMechE Vol. 221 Part G: J. Aerospace Engineering*, **2007**
[28] J. Terzic, B. Zecevic, M. Baskarad, A. Catovic, S. Serdarevic-Kadic: Prediction of Internal Ballistic Parameters of Solid Propellant Rocket Motors, *Problems of Mechatronics - Armament, Aviation, Safety Engineering*, 4(6),2011,7-26, ISSN 2081-5891